Effect of Substituents in Mussel-inspired Surface Primers on their Oxidation and Priming Efficiency

Karuppasamy Ganesh,[a] Jaewon Jung,[a] Jun Woo Park,[a] Byeong-Su Kim,[b] and Sungbaek Seo*[a]

Marine mussels contain an abundant catechol moiety, 3,4-dihydroxyphenylalanine (DOPA), in their interfacial foot proteins. DOPA contributes to both surface adhesion and bridging between the surface and overhead proteins (surface priming) by taking advantage of the unique redox properties of catechol. Inspired by the mussel surface priming mechanism, herein we synthesized a series of DOPA-mimetic analogs – a bifunctional group molecule, consisting of a catechol group and an acrylic group at the opposite ends. The surface primers with differently substituted (–COOH, $–CH_3$) alkyl chains in the middle spacer were synthesized. Time-dependent oxidation and redox potentials of the surface primers were studied in an oxidizing environment to gain a better understanding of the mussel's redox chemistry. The thickness and degree of priming of the surface primers on silicon-based substrates were analyzed by ellipsometry and UV/Vis absorption spectroscopy. The post-reactivity of the acrylic groups of the primed layer was first visualized through a reaction with an acrylic group-reactive dye.

1. Introduction

Controlling surface functionalization is essential for constructing and utilizing composite materials.[1–5] In particular, failure at the interface of the composite materials frequently occurs because of the weak adhesion between two or more materials. Acrylate-based resins are widely used as surface adhesives in composite materials because of their tunable bonding strength, design flexibility, and durability. For these reasons, it has been used in a variety of biological applications requiring composite materials such as dental fillings (BeautiBond®, Scotchbond™ Multi-Purpose®, RelyX™ U200 Automix),[6–8] artificial human-like skin constructs,[9] 3D-printable soft tissue substitutes,[10] and antimicrobial coatings.[11] The main drawback of acrylate resins is that they are made from toxic compounds and come from expensive petroleum sources.[12,13] Because acrylate resins are irreversibly cross-linked, they cannot be fixed after mechanical damage.[14] In addition, the strong adhesion of acrylate resins underwater is challenging for biomedical applications.[15,16] Therefore, the development of cost-effective, non-toxic, and strong surface adhesives with the functionality of interfacial bridging underwater is highly necessary.

Adhesion observed in nature, such as the adhesion of marine mussels on a wet rock surface, has inspired us to mimic bioadhesives by investigating the correlation between their chemical structure and adhesive properties.[17–22] 3,4-Dihydroxyphenylalanine (DOPA) is an abundant amino acid, found in the byssal plaque of a mussel, which has a catechol functionality that contributes to interfacial surface adhesion. Therefore, researchers have synthesized DOPA-mimetic small molecules or polymers for surface coating and functionalization.[23–29] The adhesive properties of these catecholic materials mainly depend on the configuration of the vicinal diol in the catechol ring, and the cohesive property of the catechol materials relies on the oxidation of catechol. Surface modification using DOPA-mimetic molecules is utilized in surface-initiated polymer grafting, cell adhesion, and patterning.[30,31] DOPA-mimetic molecules are easily oxidized under atmospheric conditions, but the mechanism of their oxidation is quite complex and not yet fully understood. In general, DOPA-mimetic molecules can be self-polymerized or cross-linked on the surface of diverse substrates in terms of oxidative catechol groups.[32]

Therefore, the investigation how the substituents in the catecholic molecules influence the oxidation and general properties is critically important. The introduction of a substituent (–Cl, $–NO_2$) in the catechol ring or a substituent (–COOH, –OH, $–CH_3$) in the alkyl chain of catecholamine strongly affects the oxidation of catechol, which promotes subsequent cross-linking reactions.[33] Catechols with electron-withdrawing groups (–COOH, –Cl, $–NO_2$) are more resistant to oxidation and promote interfacial adhesion to metal oxide surfaces. On the other hand, electron-donating group-substituted (–OH, $–CH_3$) catechols are more prone to oxidation, encouraging cohesion through oxidation product cross-linking. Therefore, the properties of the substituents influence the oxidation property of catechol, which subsequently affects its

[a] Dr. K. Ganesh, J. Jung, J. Woo Park, Prof. Dr. S. Seo
Department of Biomaterials Science (BK21 FOUR Program)
College of Natural Resources and Life Science/Life and Industry Convergence Research Institute
Pusan National University
Miryang 50463 (Republic of Korea)
E-mail: sbseo81@pusan.ac.kr
[b] Prof. Dr. B.-S. Kim
Department of Chemistry
Yonsei University
Seoul 03722 (Republic of Korea)

Supporting information for this article is available on the WWW under https://doi.org/10.1002/open.202100158

adhesive and cohesive properties as well as its applications.[34] The covalent linkage of catechol and amines (e.g., dopamine) is vital for producing coatings through cohesive forces (e.g., polydopamine).[35]

In our previous study, a DOPA-mimetic surface primer (SP), a small molecule with a catechol group on one side and an acrylate group on the opposite side with an alkyl chain spacer, was developed for the surface treatment of composite materials.[36,37] SPs are beneficial for surface adhesion with catechol groups and are further cross-linkable with acrylate groups towards another acrylate resin layer. Herein, we aim to identify the critical role of the chemical moieties in the modulation of the oxidation and priming efficiency of the SPs. By interpretation of the correlation between chemical structure and their adhesion performance, this study would provide insight into the molecular principles of self-assembled adhesion on substrates, the efficiency of priming, and the capacity of post-reaction onto the primed layer. For this purpose, a series of catecholic derivatives is synthesized, including different substituents (–COOH and $-CH_3$) in the alkyl chain spacer.

Three catecholic molecules of dopamine derivatives (D_1-D_3, D_s) and three primers (SP_1-SP_3, SP_s) were applied as follows: D_1: dopamine, D_2: dopamine with one substituent (–COOH) in the alkyl chain spacer, D_3: dopamine with two substituents (–COOH and $-CH_3$) in the alkyl chain spacer; SP_1: dopamine-derived surface primer, SP_2: surface primer with one substituent (–COOH) in the alkyl chain spacer, SP_3: dopamine with two substituents (–COOH and $-CH_3$) in the alkyl chain spacer. The oxidation kinetics of D_s and SP_s in aqueous solution were monitored, and oxidized chemical structures were suggested based on their UV/Vis absorption spectra. The oxidation and reduction potentials of D_s and SP_s were measured by cyclic voltammetry and their values were compared. The priming thickness and degree of priming on silicon-based substrates were measured using ellipsometry and UV/Vis absorption spectroscopy, respectively. After optimizing the priming efficiency through the combination of SP_s with D_s, we visually determined whether the surface-primed layers of D_s and SP_s would display reactivity for post-conjugation with an acrylic group-reactive thiol group-containing dye which is a model for biomolecules containing functional groups.

2. Results and Discussion

Substitutions in the catechol ring or alkyl chains of catecholamines have been established to influence the oxidation properties and applications of these molecules. For instance, nitrocatechols have better electron delocalization than unsubstituted catechols when they bind to Fe^{2+} and are efficiently adsorbed on Fe_3O_4 surfaces.[38] Dopamine with a methoxy substituent in the catechol ring (D1–OCH_3) is oxidized and polymerized more readily than dopamine (D_1) due to the electron-donating effect of the methoxy group. As a result, a poly(D_1–OCH_3) coating on a silicon wafer surface reduces Ag^+ to Ag nanoparticles in the same way as poly(D_1), but at a faster coating rate with the same thickness.[39] Catecholamine-poly (ethylene glycol) (PEG) gels with different substituents on the catechol ring/alkyl chain were used to prepare tissue glues.[33] The chloro (–Cl) substituent on the catechol ring, which is electron-withdrawing but π electron-donating, resulted in a faster and more efficient cross-linking, while the strong electron-withdrawing nitro group ($-NO_2$) had the opposite effect. Combining the appropriate quick and slow cross-linking catecholamine-PEG gels resulted in the development of a surgical sealant with gluing capabilities.[33] The chemical structures of levodopa (L-3,4-dihydroxyphenylalanine, D_2) and norepinephrine (NE) are similar to D_1, with the exception that D_2 has one more carboxylic group (–COOH) and NE has one more hydroxyl group (–OH) in its ethyl chain (i.e., alkyl chain substitution). The mechanism of coating of the catecholamines (D_1/D_2/NE) on a 316 L SS substrate (stainless steel, a biomaterial widely used in artificial hip joints) proceeds through different intermediates because of the alkyl chain substitution, resulting in different physical, chemical, and biological properties with various applications.[26,40]

As a result, we attempted to compare the oxidation properties and priming efficiencies of our synthesized SP_s with those of commercially available catecholamines (D_s) with differently substituted groups (ethyl chain substituents) (Figure 1a). To demonstrate the post-reactivity of the SP_s priming layer, we designed an experiment in which a fluorescent dye containing a thiol group could selectively react with the primed layer under a photomask, producing patterned fluorescent images (Figure 1b). SP_s with differently substituted groups were synthesized using a one-step process (synthetic routes in Figure S1, Supporting Information) by reacting the corresponding catecholamine (D_s) with acryloyl chloride at 80% yield. The chemical structures and molecular weights of the SP_s were confirmed through respective NMR and mass spectra (Figures S2 and S3).

The oxidation mechanism and polymerization/cross-linking behavior of D_s and SP_s were investigated by monitoring time-dependent UV/Vis absorption spectra through the addition of the oxidant $NaIO_4$ in distilled (DI) water or methanol (Figures 2, 3, and Figure S5). The UV/Vis absorption spectra of D_s and SP_s in DI water showed a characteristic peak at 281 nm, representing the symmetry-forbidden transition of the catechol group.[41,42] Upon addition of $NaIO_4$ to the D_1 solution, a new absorption maximum appeared at $\lambda = 300$ and 475 nm, corresponding to the formation of orange-colored dopaminochromes (Figure 2a).[41,43] The oxidation of D_1 in DI water under $NaIO_4$ proceeds through intramolecular cyclization, Michael-type conjugated addition, isomerization, and a free radical reaction mechanism. In the oxidation studies of D_2 and D_3, a similar spectral change was observed (Figures 2b and 2c). The time-dependent absorbance study at fixed wavelengths of 281, 300, and 475 nm also indicates that D_1 undergoes faster oxidative polymerization than D_2 and D_3, particularly between 120 min and 24 h (Figures 2d–f).

Upon oxidation of SP_1, the intensity of the peak at 281 nm decreased immediately, and a new peak was formed at 395 nm which corresponds to the formation of dopaquinone (Figure 3a). The resulting yellow-colored dopaquinone disappeared

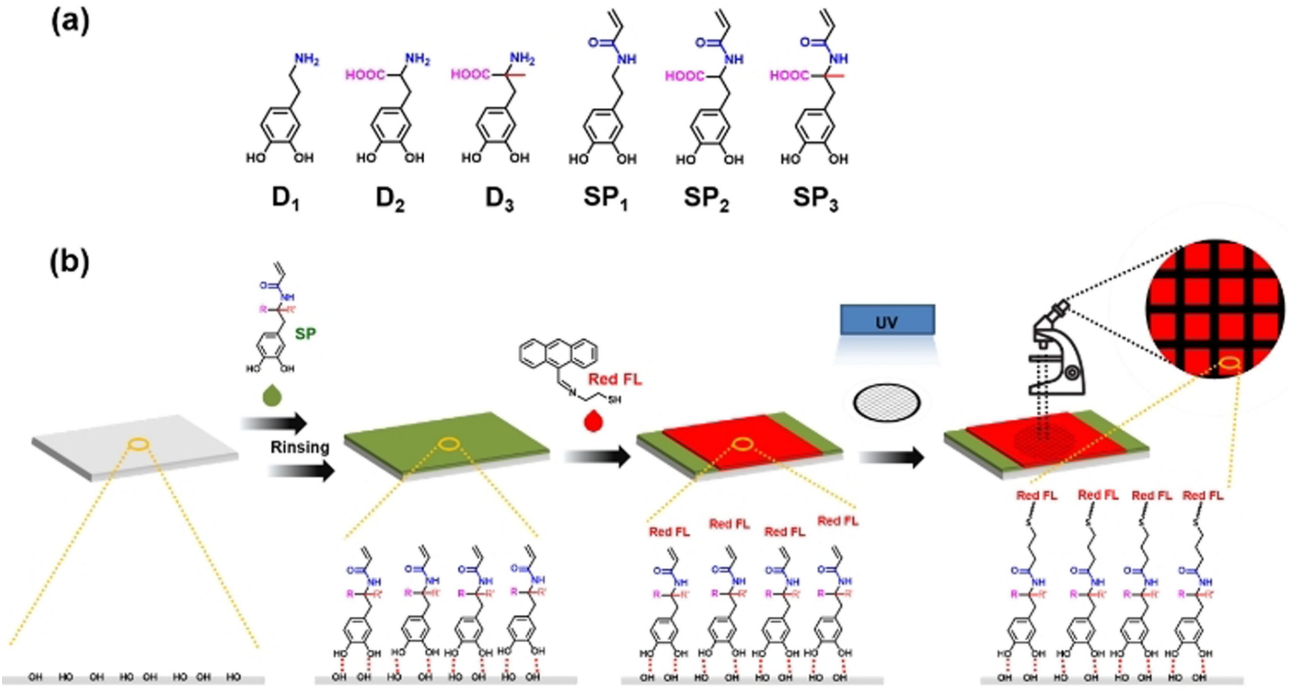

Figure 1. (a) Catecholic molecules used for surface priming: Dopamine derivatives (D_1-D_3, D_s) and surface primers (SP_1-SP_3, SP_s) based on parent compound of D_s. (b) A schematic procedure for demonstrating reactivity of the SP_s priming layer. The primed layer is reacted with red fluorescent acrylic group-reactive dye under a patterned mask with UV irradiation.

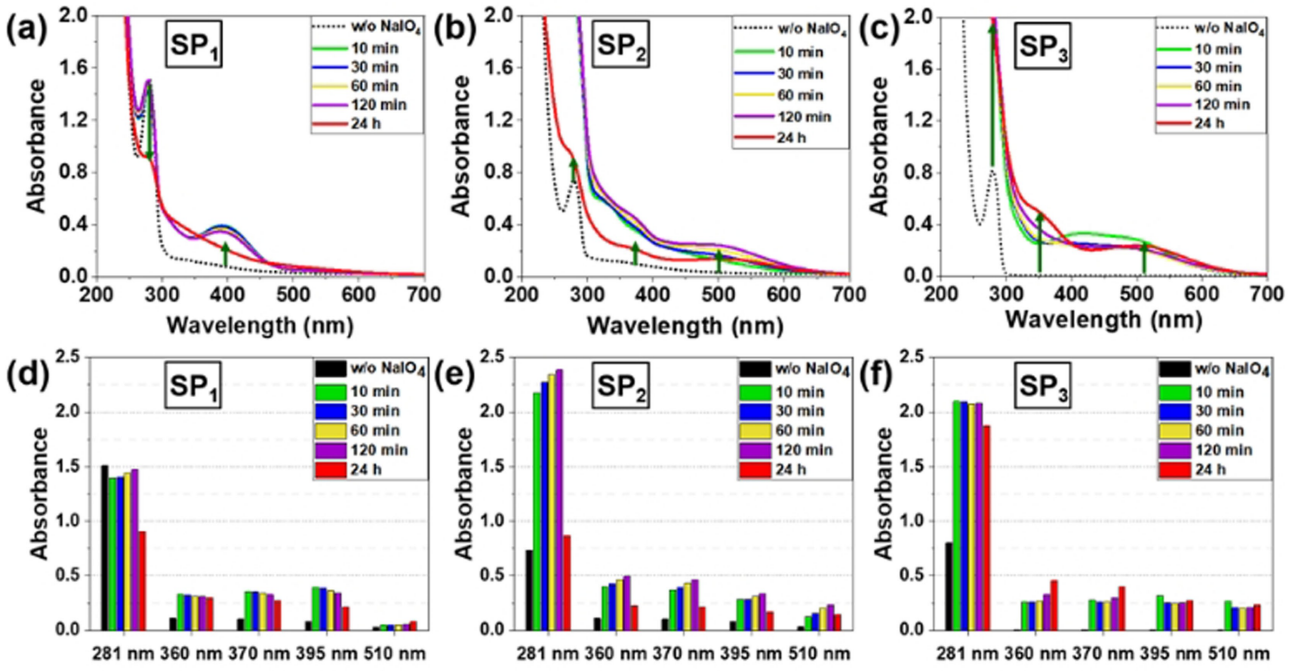

Figure 2. Time-dependent oxidation studies of (a–c) D_s (5×10^{-4} M) in distilled water with $NaIO_4$ (5×10^{-4} M). (d–f) Comparison of absorption intensity of all samples at fixed wavelengths

instantaneously and a new intermediate was formed with time, resembling the insect cuticle sclerotization process.[44] It has been reported that the oxidation of *N*-acetyl dopamine does not involve cyclization to the 5,6-dihydroxyindole intermediate; instead, it undergoes oxidative and cross-linking pathways.[33] Therefore, we expected that the reaction pathway, which is similar to the *N*-acylated dopamine, takes place in SP_1 because it also lacks the primary amine functionality, which is connected to the acrylate cross-linking unit by an amide bond.

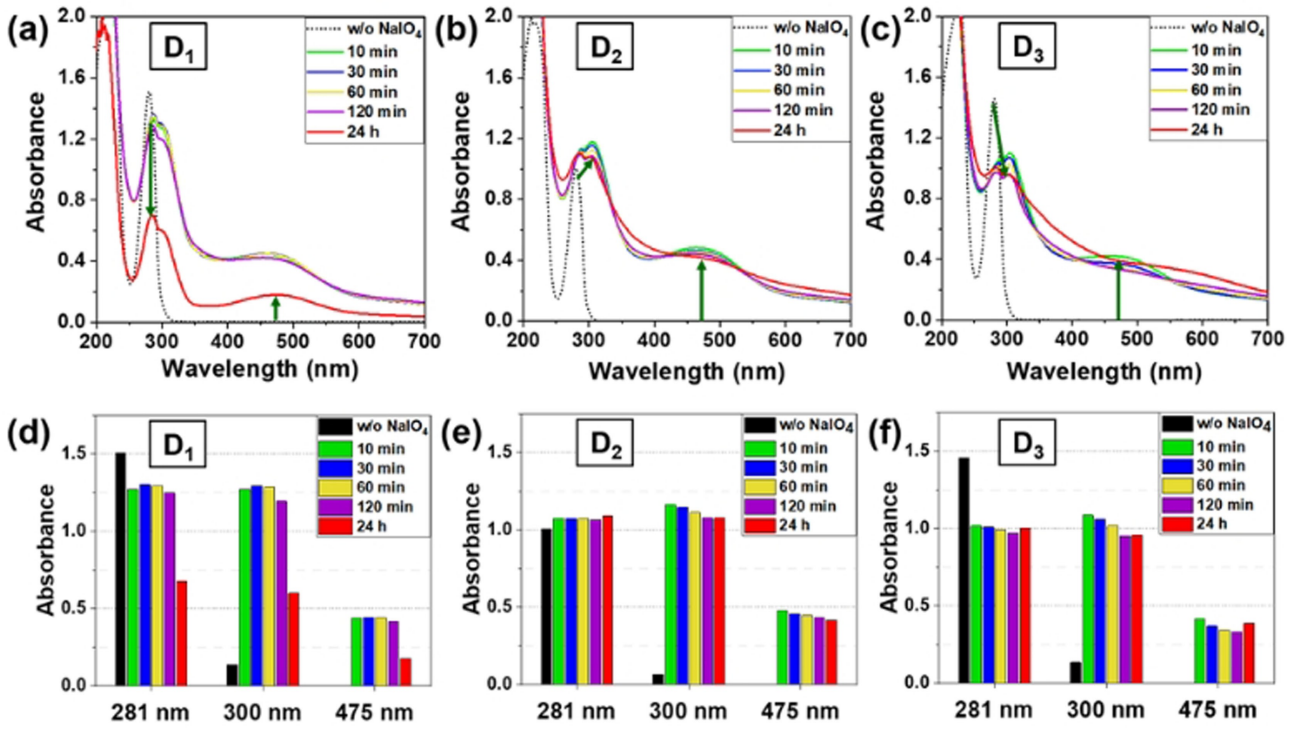

Figure 3. Time-dependent oxidation studies of (a–c) SP_s (5×10^{-4} M) in distilled water with $NaIO_4$ (5×10^{-4} M). (d–f) Comparison of absorption intensity of all samples at fixed wavelengths

Oxidation studies of SP_2/SP_3 showed a characteristic dopaquinone peak at 395 nm, which decreased instantaneously, and a new weak and broad peak at 510 nm was formed (Figures 3b and 3c). In addition, a new band was formed at 370 and 360 nm for SP_2 and SP_3, indicating the formation of 6,7-dihydroxyhydrocoumarin (dihydroesculetin) derivatives resulting from the instantaneous intramolecular cyclization reaction of dopaquinone and the carboxylate anion.[45] It has been reported in the literature that the peak above 500 nm suggests the formation of a hydroxyquinone chromophore from the hydrolysis of 6,7-dihydroxy hydrocoumarin.[33] Similar transient species were formed during the spectral studies of hydrocaffeic acid, and the SP_2 molecule further confirmed the same mechanistic pathway of the polymerization reaction (Figure S4). The time-dependent absorbance study at fixed wavelengths (particularly at 281 and 510 nm) also indicates that SP_1 as well as SP_2 and SP_3 react through a different mechanism (Figures 3d–f). The kinetic oxidation study, changing the solvent from DI water to methanol in the SP solution, supported a different mechanistic pathway of oxidation, as mentioned in the literature (Figure S5).[35] In the case of SP_1 oxidation, it resulted in the formation of a characteristic oligomer (e.g., coupling of phenol and quinone) through dopaquinone which has characteristic peaks at 420 and 390 nm, respectively (Figure S5–1). The presence of a carboxyl group at the α-carbon and a hydrogen at the β-carbon of SP_2 induced the formation of an α,β-dehydro-DOPA acetyl derivative intermediate, which has a characteristic peak at 320 nm (Figure S5–2). However, the hydrogen at the α-carbon of SP_3, which was replaced by a methyl group, resulted in the formation of a quinone methide intermediate (Figure S5–3). The formation of the oligomer, of the α,β-dehydro-DOPA acetyl derivative, and of the quinone methide intermediates from SP_1, SP_2, and SP_3, respectively, in the polymerization/oxidation mechanism are due to the differences in the substituted groups of the α-carbon atom of the SP_s. Eventually, the solvent methanol itself acts as a nucleophile and reacts with the formed dopaquinone intermediate to form a substituted ether, which is a Michael-addition product. These ethers were further oxidized to methoxy orthoquinones, which had a characteristic peak above 500 nm. The substituents at the α-carbon of the SP_s resulted in the formation of various intermediates during the oxidative polymerization. In particular, SP_2 formed an intramolecular cyclized 6,7-dihydroxyhydrocoumarin intermediate in water, and the α,β-dehydro-DOPA derivative in methanol might account for the decrease in the number of reactive sites for cross-linking and eventual polymerization.[33,46] Thus, a slow-cross-linking adhesive primer such as SP_2 could act as a sealant in surgery, cell encapsulation, and cell therapies.[47]

To evaluate their redox potential, electrochemical studies of SPs and their parent compounds (D_s) were conducted (Figure 4 and Table 1). In the case of D_1, a redox pair with a peak anodic potential (E_{pa}) of 0.5848 V and a peak cathodic potential (E_{pc}) of 0.2917 V versus Ag/AgCl was detected, which is consistent with previously reported values.[48] The potential peak difference of D_s ($\Delta E = E_{pa}$-E_{pc}) is approximately 300 mV, indicating that these reactions are not reversible and that they follow the mechanistic sequence including an initial two electron oxidation to a

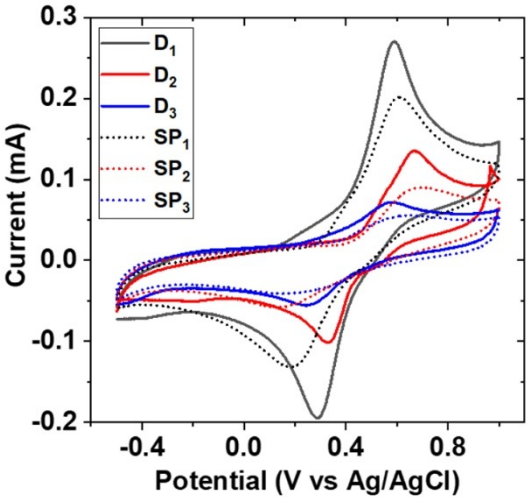

Figure 4. Cyclic voltammograms of D_s (1 mM) and SP_s (1 mM) solution in 1 M NaCl aqueous solution as a supporting electrolyte at a scan rate of 300 mV s^{-1}.

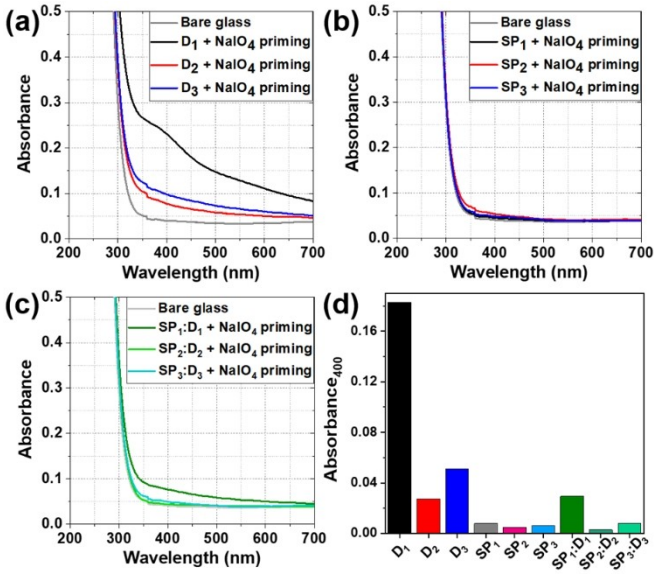

Figure 5. (a–c) UV/Vis absorption spectra of the priming layer of (a) D_s, (b) SP_s, (c) SP_s:D_s on glass slide. (d) Absorption intensity at 400 nm of priming layer of D_s, SP_s and SP_s:D_s (5:1 molar ratio) on glass slides.

Table 1. Anodic potential (E_{pa}), cathodic potential (E_{pc}), and potential peak difference ($\Delta E = E_{pa}$-E_{pc}) of D_s and SP_s

Compound	E_{pa} [V]	E_{pc} [V]	ΔE [V]
D_1	0.5848	0.2917	0.2931
D_2	0.6621	0.3373	0.3248
D_3	0.5756	0.2474	0.3282
SP_1	0.6090	0.1950	0.4140
SP_2	0.6859	0.1462	0.5397
SP_3	0.6127	0.1847	0.4280

quinone, which is then rapidly cyclized to the 5,6-dihydroxyindole and a chemical redox transfer.[49]

A considerable shift towards positive potential was observed for the SP_s containing acrylic groups compared to their parent compounds (D_1:0.5848 V→SP_1:0.6090 V; D_2:0.6621 V→SP_2: 0.6859 V; D_3: 0.5756 V→SP_3:0.6127 V), which are comparable to those of dopamine and its methylated derivatives.[48] Thus, the attachment of an acrylic group to the catecholamines made them relatively resistant to oxidation. D_2 exhibits a higher anodic oxidation potential E_{pa} (0.6621 V) when compared to D_1 (0.5848 V; α-H) and D_3 (0.5756 V; α–COOH/α′–CH_3 groups). The modification of nucleophilicity (the presence of the α-COOH group) in the side chain may induce toxicity in biological environments.[50]

Ellipsometry was performed to evaluate the priming thickness of D_s and SP_s on a silicon wafer substrate (Figure S6). It was confirmed that the covalent attachment of catechol and amine (i.e., in the case of D_s) resulted in a better coating performance than the corresponding SP_s. These findings also verified the effect of the substituted group on the coating performance, which was in the order of $D_1 > D_3 > D_2 > SP_1 > SP_3 > SP_2$. To compare the degree of priming of D_s and SP_s, the absorption of both D_s and SP_s primed on glass slides were measured using UV/Vis absorption spectroscopy. As shown in Figure 5a, D_s priming showed broadband spectra around 400 nm, whereas SP_s priming showed spectra similar to blank glass (Figure 5b). As expected, both D_2 and D_3 can self-polymerize to form priming on a glass surface under oxidative conditions (alkaline pH or the use of $NaIO_4$ as an oxidant), as D_1 does. D_2 and D_3 formed a weaker priming in comparison with D_1 by forming soluble, melanin-like intermediate products or non-precipitating supramolecular nanoaggregates.[44,51] The impressive priming ability of D_s in the order $D_1 > D_3 > D_2$ may be due to intermolecular covalent linking between the free primary amine and catechol. A weak, thin, or no priming was observed in the case of SP_s. Our explanation is that the primary amine functionality of D_s was lost, resulting in the prevention of self-oxidation polymerization; therefore, they could mostly form self-assembled monolayers (SAMs) on variable substrates.[32,52,53]

Co-deposition of D_s and SP_s, for example, SP_1 blended with the corresponding D_1 (SP_1:D_1), was applied to boost the priming efficiency of SP_1, as it provided the primary amine functionality (nucleophile) and helped create 5,6-dihydroxyindole that played a dual role in initiating the coating process and acted as a 'cross-linker' in the formation of a polydopamine-like coating.[53] The priming on the glass substrate through the co-deposition method was also measured using UV/Vis absorption spectroscopy, confirming the enhancement of the degree of priming in the order of (SP_1:D_1) > (SP_3:D_3) > (SP_2:D_2) (Figures 5c and 5d).

To visualize the effectiveness of the priming and the availability of a post-conjugation step, a thiol-ene click reaction was performed on the primed glass slides. An anthraldehyde disulfide (Dye-S-S-Dye) was synthesized, which could be reduced in situ to generate a free thiol-containing dye (Dye-SH) and subsequently reacted with the primed glass substrate through a thiol acrylate-radical pathway. The primed glass containing a catechol and an acrylamide functionality was conjugated to the in situ-generated free thiol dye ND showed

strong fluorescence in the 350 nm region, in which the chromophore fluoresces.[54]

Comparisons were carried out with D_s, SP_s, and co-depositions of SP_s:D_s priming. After priming, the glass substrates were thoroughly rinsed with methanol to remove any remaining unbound primers. The fluorescent dye was then applied to the primed substrate, and a cross-section-patterned grid was placed on the dye-primed glass surface to enable the thiol-ene click reaction to occur with irradiation, resulting in a fluorescent pattern.

The fluorescent pattern of D_s priming was observed using fluorescence microscopy images (Figure 6). It seems that the covalent coupling/Michael-addition reaction between catechol/quinone groups was present in the polydopamine-like coating with the nucleophilic thiol dye.[55–57] Relatively poor and scattered fluorescence patterns were observed in the case of SP_s priming because they formed SAMs instead of coatings on the glass substrate. Therefore, non-uniform SAMs were less reactive to the available fluorescent dye. A stronger and clearer fluorescence pattern was observed for the co-deposition technique priming, since it formed a strong priming on the glass substrate. As a result, a well-defined covalent coupling/Michael-addition reaction took place between the catechol/quinone and acrylamide groups present in the co-deposition technique priming with the nucleophilic thiol dye as suggested in Figure 7.[55–57]

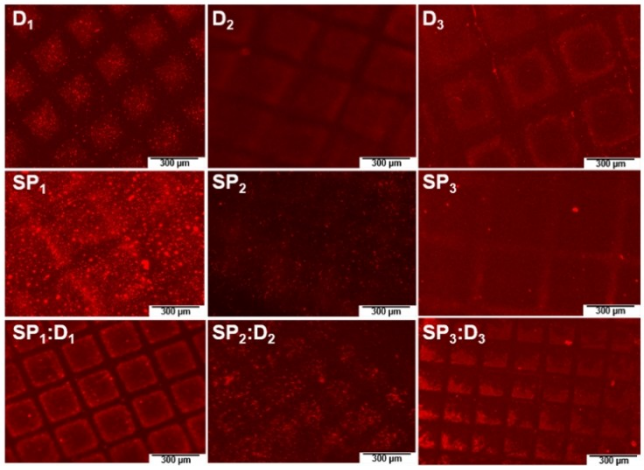

Figure 6. Fluorescence microscopy images of surface-primed glass after post-conjugation with red fluorescent thiol group-containing dye under a patterned mask. The surfaces are primed by D_s, SP_s, and a co-deposition of SP_s:D_s (5:1 molar ratio).

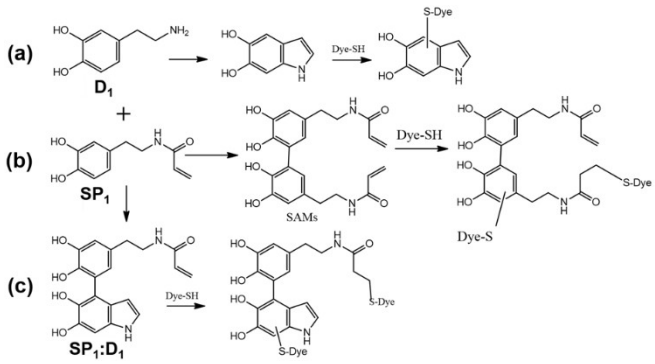

Figure 7. Plausible chemical species that formed on the glass slides during the surface priming of (a) D_1, (b) SP_1, and (c) co-deposition of SP_1:D_1.

3. Conclusion

DOPA-mimetic surface primers with different substituents were synthesized and characterized, and their priming efficiencies were investigated. UV/Vis absorption spectroscopy and cyclic voltammetry were used to describe the possible oxidative cross-linking properties of the surface primers. With the co-deposition of the surface primers and primary amine-containing catechol molecules, their priming capability was improved. Priming was first visualized in regulated patterns with dye labeling after the post-reaction on the primed layer on the glass slides. This study will provide insight to develop wet-adhesives and catecholic materials for demanding post-conjugation chemistry and interfacial engineering in composite materials.

Experimental Section

Materials

Acryloyl chloride (97%) was distilled under reduced pressure and stored under an argon atmosphere. 2-(3,4-Dihydroxyphenyl) ethylamine hydrochloride (D_1, 98%), 3,4-dihydroxy-L-phenylalanine (D_2, $\geq$98%), (−)-3-(3,4-dihydroxyphenyl)-2-methyl-L-alanine sesquihydrate (D_3, 99%), cystamine dihydrochloride (96%), 9-anthraldehyde (97%), tris(2-carboxyethyl) phosphine hydrochloride (TCEP, 98%), sodium tetraborate decahydrate ($Na_2B_4O_7 \cdot 10H_2O$), sodium carbonate (Na_2CO_3), magnesium sulfate ($MgSO_4$), sodium chloride (NaCl), and anhydrous calcium chloride ($CaCl_2$) were of the highest grade and were purchased from Sigma Aldrich (USA) and used without further purification. 2,2-Dimethoxy-2-phenylacetophenone (DMPA, 98%) was purchased from TCI Chemicals (Japan). Deuterated DMSO-d_6, deuterium oxide, and methanol-d_4 were purchased from Cambridge Isotope Laboratories, Inc. (USA).

Synthesis of SP_1-SP_3 and Anthracene Schiff-Base Dye (Dye-S-S-Dye)

N-*(3,4-Dihydroxyphenethyl) acrylamide (SP_1)*

A modified procedure was adopted from Detrembleur et al.[58,59] A two-neck round-bottom flask was charged with 12.1 g (31.6 mmol) of $Na_2B_4O_7 \cdot 10 \cdot H_2O$ and 5.0 g of Na_2CO_3 and 475 mL of Milli-Q water (18.2 MΩ cm). This basic aqueous solution was degassed in a sonicator bath (Nexul NXP 1002, 100 W, 40 kHz) for 1 h, followed by argon bubbling for another 2 h. 3 g (15.8 mmol) of D_1 were added under an argon atmosphere and allowed to continue stirring for 30 min. The flask was then cooled to 0 °C before the dropwise addition of 5.1 mL (63.2 mmol) of acryloyl chloride with stirring. Then 9.0 g of Na_2CO_3 were added to maintain the pH of the solution above 9.0 during the reaction. After stirring for 12 h at 23 ± 2 °C, the solution was acidified to pH 1-2 with 6 N HCl and stirred continuously for 1 h in an open vessel. The mixture was extracted five times with ethyl acetate, washed twice with 0.1 M

HCl, and dried over $MgSO_4$. The solvent was removed in a vacuum to yield a crude grayish paste, which was further purified by flash silica gel column chromatography and eluted with a dichloromethane–methanol (9:1) mixture (white solid, 80% yield).

2-Acrylamido-3-(3,4-dihydroxyphenyl) propanoic acid (SP_2)

The same protocol was followed, in which D_1 was replaced with D_2. (pale yellow resin, 80% yield)

2-Acrylamido-3-(3,4-dihydroxyphenyl)-2-methylpropanoic acid (SP_3)

The same protocol above was followed, in which D_1 was replaced with D_3. (ash powder, 80% yield).

Anthracene Schiff-Base Dye (Dye-S-S-Dye)

A modified procedure was employed for the synthesis of an anthracene Schiff-base dye (Dye-S-S-Dye) containing a disulfide.[60] 9-Anthraldehyde (1.0 g, 4.8 mmol) and 2–2′-diaminodiethyl disulfide dihydrochloride (0.544 g, 2.4 mmol) were mixed in dry methanol (20 mL) in the presence of triethylamine (0.490 g, 4.8 mmol) and the mixture was refluxed at 60 °C for 12 h under a nitrogen atmosphere. The reaction mixture was cooled, and the solvent was evaporated to give the crude product, which was recrystallized from a dichloromethane/ethanol mixture to produce a pure compound (yellow powder, 90% yield).

The synthesized primers (SP_1-SP_3) and Dye-S-S-Dye were stored in a desiccator filled with $CaCl_2$ for later use.

UV/Vis Absorption Spectroscopy Studies of the D_s and SP_s Solutions

Respective D_s/SP_s (1 mM) were dissolved in distilled water (DI water) or methanol and then mixed with $NaIO_4$ (1 mM) in DI water at a 1:1 volume ratio. The UV/Vis absorption spectra of the D and SP solutions were recorded at 23 ± 2 °C using a UV/Vis spectrophotometer (Biochrome Libra S50, UK) in DI water or methanol before and after the addition of the oxidant $NaIO_4$ according at predetermined incubation times (10, 30, 60, 120 min, and 24 h).

Cyclic Voltammetry (CV) of D and SP Solutions

CV measurements of the D and SP solutions were performed using a Versastat 3 potentiostat (Ametek Co., USA). These analyses were conducted using a three-electrode cell with a Pt wire as the counter electrode, an Ag/AgCl reference electrode, and a glassy carbon electrode as the working electrode. Electrochemical analyses of the D and SP solutions (1 mM) were recorded in 1 M NaCl aqueous solution as a supporting electrolyte at a scan rate of 300 mV s^{-1} at room temperature. Catechol autoxidation was avoided by performing electrochemical experiments with degassed DI water under nitrogen.

Preparation of D_s, SP_s and a Blend of D_s and SP_s (D_s:SP_s) Priming on Silicon-based Substrates

The silicon wafer substrates were sonicated in methanol for 5 min, followed by nitrogen flushing, ozone treatment, and immersion in a 1:1 (v/v) mixture of an aqueous solution of D_s/SP_2/SP_3 (10 mM, 20 mL) (methanol in the case of SP_1) and an aqueous solution of $NaIO_4$ (10 mM, 20 mL). After 24 h, the priming substrates were rinsed with methanol, deionized (DI) water, and dried under nitrogen. The thickness of the priming on the silicon wafer was measured by spectroscopic ellipsometry at an angle of incidence of 70° in a wavelength (λ) range of 400–700 nm (alpha-SE, J.A. Woollam, USA) using the Cauchy model.

For priming onto glass slides with D_s/SP_s, we prepared primer solutions by dissolving D_s (2 mM)/SP_s (10 mM) with the corresponding equivalent moles of the oxidant $NaIO_4$ (2 mM or 10 mM, respectively) in DI water (or methanol, in the case of SP_1). For priming onto glass slides with D_s:SP_s, the following primer solution was prepared: 4 mM D_s/20 mM SP_s as a mixture were dissolved in 10 mL DI water (methanol in the case of SP_1), and a 24 mM $NaIO_4$ solution was separately added to 10 mL of DI water. Then, 5 mL of each sample was mixed to generate a primer solution. Accordingly, the molar ratio of SP_s:D_s was 5:1, and the primer mixture and oxidant were 1:1. The ozone-treated glass slides were immersed in this solution for 24 h at room temperature, the glass slides were cleaned in DI water and dried with nitrogen gas. The degree of priming by D_s/SP_s/SP_s:D_s on glass slides was measured using UV/Vis absorption spectra.

Post-Reaction of Fluorescent Dyes onto Primed Glass Slides

Immediately before the post-reaction onto the priming (D_s/SP_s/SP_s:D_s) of glass slides, Dye-S-S-Dye (0.002 g, 0.0029 mmol) was added to a round-bottom flask containing DMF (1 mL) and a stir bar. TCEP (0.0012 g, 0.0044 mmol) was added, and the reaction was allowed to proceed for 30 min to reduce and generate a thiol functional dye (Dye-SH). This in situ-generated Dye-SH solution was carefully added to the primed glass slides along with the photoinitiator DMPA (0.0011 g, 0.0044 mmol). Then, a transmission electron microscopy copper grid was placed over the glass surface, which was irradiated under a 350 nm UV lamp (233 mW cm^{-2}, distance of 1 cm) for 5 min. The glass slides were washed with DMF and dried under nitrogen. The pattering images from the reacted fluorescent dye were examined using optical/fluorescence microscopy (Eclipse TS100, Nikon).

Acknowledgements

This work was supported by a National Research Foundation of Korea (NRF) grant funded by the Korean government (MSIP: Ministry of Science, ICT & Future Planning) (NRF-2018R1D1A1B07050070, 2021R1F1A105923711 and NRF-2021R1A2C3004978) and the BK21 FOUR Program through the National Research Foundation of Korea (NRF) funded by the Ministry of Education, Korea (F21YY8109033).

Conflict of Interest

The authors declare no conflict of interest.

Keywords: acrylamide · catechol · priming efficiency · substituent effect · surface primer

[1] S. A. Pendergraph, M. D. Bartlett, K. R. Carter, A. J. Crosby, *ACS Appl. Mater. Interfaces.* **2012**, *4*, 6640–6645.
[2] M. Guttag, M. C. Boyce, *Adv. Funct. Mater.* **2015**, *25*, 3641–3647.

[3] G. Ranjith Kumar, G. Rajyalakshmi, V. Kumar Manupati, *Mater. Today Proc.* **2018**, *5*, 6963–6972.
[4] M. Xie, G. Lin, D. Ge, L. Yang, L. Zhang, J. Yin, X. Jiang, *ACS Mater. Lett.* **2019**, *1*, 77–82.
[5] V. Narayanamurthy, F. Samsuri, A. Y. Firus Khan, H. A. Hamzah, M. B. Baharom, T. V. Kumary, P. R. Anil Kumar, D. K. Raj, *Bioinspir. Biomim.* **2019**, *15*, 016002.
[6] S.-B. Lee, C. González-Cabezas, K.-M. Kim, K.-N. Kim, K. Kuroda, *Biomacromolecules* **2015**, *16*, 2265–2275.
[7] D. Lee, H. Bae, J. Ahn, T. Kang, D.-G Seo, D. S. Hwang, *Acta Biomater.* **2020**, *103*, 92–101.
[8] T. T. Fröhlich, T. L. Lenzi, F. Z. M. Soares, R. de. O. Rocha, *Int. J. Adhes. Adhes.* **2021**, *107*, 102862.
[9] Z. Zhang, L. Wang, H. Yu, F. Zhang, L. Tang, Y. Feng, W. Feng, *ACS Appl. Mater. Interfaces* **2020**, *12*, 15657–15666.
[10] F. Asai, T. Seki, A. Sugawara-Narutaki, K. Sato, J. Odent, O. Coulembier, J.-M. Raquez, Y. Takeoka, *ACS Appl. Mater. Interfaces* **2020**, *12*, 46621–46628.
[11] Q. Cheng, A. B. Asha, Y. Liu, Y.-Y. Peng, D. Diaz-Dussan, Z. Shi, Z. Cui, R. Narain, *ACS Appl. Mater. Interfaces* **2021**, *13*, 9006–9014.
[12] R. M. O'Dea, J. A. Willie, T. H. Epps, *ACS Macro Lett.* **2020**, *9*, 476–493.
[13] C. Veith, F. Diot-Néant, S. A. Miller, F. Allais, *Polym. Chem.* **2020**, *11*, 7452–7470.
[14] G. Fortunato, E. Tatsi, B. Rigatelli, S. Turri, G. Griffini, *Macromol. Mater. Eng.* **2020**, *305*, 1900652.
[15] B. P. Lee, P. B. Messersmith, J. N. Israelachvili, J. H. Waite, *Annu. Rev. Mater. Res.* **2011**, *41*, 99–132.
[16] K. T. Tan, C. C. White, D. L. Hunston, C. Clerici, K. L. Steffens, J. Goldman, B. D. Vogt, *J. Adhes.* **2008**, *84*, 339–367.
[17] P. M. Favi, S. Yi, S. C. Lenaghan, L. Xia, M. Zhang, *J. Adhes. Sci. Technol.* **2014**, *28*, 290–319.
[18] O. Pinkas, D. Goder, R. Noyvirt, S. Peleg, M. Kahlon, M. Zilberman, *Acta Biomater.* **2017**, *51*, 125–137.
[19] Y. Zhao, Y. Wu, L. Wang, M. Zhang, X. Chen, M. Liu, J. Fan, J. Liu, F. Zhou, Z. Wang, *Nat. Commun.* **2017**, *8*, 2218.
[20] E. Azad, M. Atai, M. Zandi, P. Shokrollahi, L. Solhi, *Dent. Mater.* **2018**, *34*, 1263–1270.
[21] A. H. J. Gowda, Y. Bu, O. Kudina, K. V. Krishna, R. A. Bohara, D. Eglin, A. Pandit, *Int. J. Biol. Macromol.* **2020**, *164*, 1384–1391.
[22] D. W. R. Balkenende, S. M. Winkler, P. B. Messersmith, *Eur. Polym. J.* **2019**, *116*, 134–143.
[23] X. Zhang, H. Liu, L. Yue, Y. Bai, J. He, *J. Mater. Sci.* **2020**, *55*, 7981–7997.
[24] Y. K. Jeong, S. H. Park, J. W. Choi, *ACS Appl. Mater. Interfaces* **2018**, *10*, 7562–7573.
[25] H. Wang, C. Lin, X. Zhang, K. Lin, X. Wang, S. G. Shen, *ACS Appl. Mater. Interfaces* **2019**, *11*, 7615–7625.
[26] X. Tan, P. Gao, Y. Li, P. Qi, J. Liu, R. Shen, L. Wang, N. Huang, K. Xiong, W. Tian, Q. Tu, *Bioact. Mater.* **2021**, *6*, 285–296.
[27] K. Feng, L. Peng, L. Yu, Y. Zheng, R. Chen, W. Zhang, G. Chen, *ACS Appl. Mater. Interfaces* **2020**, *12*, 27632–27639.
[28] E. Shin, S. W. Ju, L. An, E. Ahn, J.-S. Ahn, B.-S. Kim, B. K. Ahn, *ACS Appl. Mater. Interfaces* **2018**, *10*, 1520–1527.
[29] E. Shin, C. Lim, U. J. Kang, M. Kim, J. Park, D. Kim, W. Choi, J. Hong, C. Baig, D. W. Lee, B.-S. Kim, *Macromolecules* **2020**, *53*, 3551–3562.
[30] X. Fan, L. Lin, J. L. Dalsin, P. B. Messersmith, *J. Am. Chem. Soc.* **2005**, *127*, 15843–15847.
[31] S. H. Ku, J. S. Lee, C. B. Park, *Langmuir* **2010**, *26*, 15104–15108.
[32] Q. Ye, F. Zhou, W. Liu, *Chem. Soc. Rev.* **2011**, *40*, 4244.
[33] J. I. Paez, O. Ustahüseyin, C. Serrano, X.-A. Ton, Z. Shafiq, G. K. Auernhammer, M. D'Ischia, A. del Campo, *Biomacromolecules* **2015**, *16*, 3811–3818.
[34] G. P. Maier, C. M. Bernt, A. Butler, *Biomater. Sci.* **2018**, *6*, 332–339.
[35] H. Hu, J. C. Dyke, B. A. Bowman, C.-C. Ko, W. You, *Langmuir* **2016**, *32*, 9873–9882.
[36] S. Seo, D. W. Lee, J. S. Ahn, K. Cunha, E. Filippidi, S. W. Ju, E. Shin, B.-S Kim, Z. A. Levine, R. D. Lins, J. N. Israelachvili, J. H. Waite, M. T. Valentine, J. E. Shea, B. K. Ahn, *Adv. Mater.* **2017**, *29*, 1703026.
[37] K. H. Park, J. Jung, S. Yim, M. J. Kang, G. Kwon, D. Y. Hwang, S. Y. Yang, S. Seo, *ChemistrySelect* **2020**, *5*, 5842–5849.
[38] E. Amstad, A. U. Gehring, H. Fischer, V. V. Nagaiyanallur, G. Hähner, M. Textor, E. Reimhult, *J. Phys. Chem. C* **2011**, *115*, 683–691.
[39] J. Zhang, Y. S. Cheah, S. Santhanakrishnan, K. G. Neoh, C. L. L. Chai, *Polymer (Guildf).* **2017**, *116*, 5–15.
[40] T. Iwasaki, Y. Tamai, M. Yamamoto, T. Taniguchi, K. Kishikawa, M. Kohri, *Langmuir* **2018**, *34*, 11814–11821.
[41] D. K. Yeon, S. Ko, S. Jeong, S.-P. Hong, S. M. Kang, W. K. Cho, *Langmuir* **2019**, *35*, 1227–1234.
[42] W. Barreto, S. Ponzoni, P. Sassi, *Spectrochim. Acta Part A.* **1998**, *55*, 65–72.
[43] M. Bisaglia, S. Mammi, L. Bubacco, *J. Biol. Chem.* **2007**, *282*, 15597–15605.
[44] A. Abebe, D. Zheng, J. Evans, M. Sugumaran, *Insect Biochem. Mol. Biol.* **2010**, *40*, 650–659.
[45] M. Sugumaran, *Int. J. Mol. Sci.* **2016**, *17*, 1576.
[46] L. M. Rzepecki, J. H. Waite, *Arch. Biochem. Biophys.* **1991**, *285*, 27–36.
[47] H. Zhang, L. Bré, T. Zhao, B. Newland, M. Da Costa, W. Wang, *J. Mater. Chem. B* **2014**, *2*, 4067.
[48] E. Nam, J. S. Derrick, S. Lee, J. Kang, J. Han, S. J. C. Lee, S. W. Chung, M. H. Lim, *ACS Chem. Neurosci.* **2018**, *9*, 2655–2666.
[49] S. Corona-Avendaño, G. Alarcón-Angeles, M. T. Ramírez-Silva, G. Rosquete-Pina, M. Romero-Romo, *J. Electroanal. Chem.* **2007**, *609*, 17–26.
[50] I. Iftikhar, K. M. A. El-Nour, A. Brajter-Toth, *ChemElectroChem* **2018**, *5*, 1056–1063.
[51] S. Moulay, *Polym. Rev.* **2014**, *54*, 436–513.
[52] J. Liebscher, *European J. Org. Chem.* **2019**, *2019*, 4976–4994.
[53] Q. Lyu, N. Hsueh, C. L. L. Chai, *Langmuir* **2019**, *35*, 5191–5201.
[54] S. Slavin, E. Khoshdel, D. M. Haddleton, *Polym. Chem.* **2012**, *3*, 1461–1466.
[55] N. Shahkaramipour, C. K. Lai, S. R. Venna, H. Sun, C. Cheng, H. Lin, *Ind. Eng. Chem. Res.* **2018**, *57*, 2336–2345.
[56] A. Vaish, D. J. Vanderah, L. J. Richter, M. Dimitriou, K. L. Steffens, M. L. Walker, *Chem. Commun.* **2015**, *51*, 6591–6594.
[57] H.-W. Chien, W.-H Kuo, M.-J. Wang, S. W. Tsai, W.-B. Tsai, *Langmuir* **2012**, *28*, 5775–5782.
[58] N. Patil, C. Falentin-Daudré, C. Jérôme, C. Detrembleur, *Polym. Chem.* **2015**, *6*, 2919–2933.
[59] Z. Zeng, H. Wang, Y. Morsi, X. Mo, *Colloids Surf. B.* **2018**, *161*, 94–102.
[60] M. Shellaiah, Y. C. Rajan, P. Balu, A. Murugan, *New J. Chem.* **2015**, *39*, 2523–2531.

Manuscript received: July 1, 2021
Revised manuscript received: August 13, 2021